2012

Assembly of uniaxially aligned rare-earth-free nanomagnets

Balamurugan Balamurugan
University of Nebraska-Lincoln, balamurugan@unl.edu

Bhaskar Das
University of Nebraska-Lincoln, bhaskar.das@huskers.unl.edu

Shah R. Valloppilly
University of Nebraska-Lincoln, svalloppilly2@unl.edu

Ralph Skomski
University of Nebraska-Lincoln, rskomski2@unl.edu

Xingzhong Li
University of Nebraska-Lincoln, xli2@unl.edu

See next page for additional authors

Assembly of uniaxially aligned rare-earth-free nanomagnets

B. Balamurugan,[1,2] B. Das,[1,2] V. R. Shah,[1] R. Skomski,[1,2] X. Z. Li,[1] and D. J. Sellmyer[1,2,a)]
[1]*Nebraska Center for Materials and Nanoscience, University of Nebraska, Lincoln, Nebraska-68588, USA*
[2]*Department of Physics and Astronomy, University of Nebraska, Lincoln, Nebraska-68588, USA*

(Received 20 July 2012; accepted 4 September 2012; published online 19 September 2012)

We report $HfCo_7$ nanoparticles with appreciable permanent-magnet properties (magnetocrystalline anisotropy $K_1 \approx 10$ Mergs/cm^3, coercivity $H_c \approx 4.4$ kOe, and magnetic polarization $J_s \approx 10.9$ kG at 300 K) deposited by a single-step cluster-deposition method. The direct crystalline-ordering of nanoparticles during the gas-aggregation process, without the requirement of a high-temperature thermal annealing, provides an unique opportunity to align their easy axes uniaxially by applying a magnetic field of about 5 kOe prior to deposition, and subsequently to fabricate exchange-coupled nanocomposites having J_s as high as 16.6 kG by co-depositing soft magnetic Fe-Co. This study suggests $HfCo_7$ as a promising rare-earth-free permanent-magnet alloy, which is important for mitigating the critical-materials aspects of rare-earth elements. © *2012 American Institute of Physics*. [http://dx.doi.org/10.1063/1.4753950]

Magnetic nanoparticles of high magnetocrystalline anisotropy $K_1 \geq 10$ Mergs/cm^3 and magnetic polarization J_s above about 10 kG ($J_s = 4\pi M_s$, M_s is the saturation magnetization) are of interest for permanent magnets, recording media, and other significant applications.[1–3] Such nanoparticle building-blocks are promising for improving magnetic properties by exploiting nanoscale effects and miniaturizing devices to suit modern technological requirements.[4,5] Rare-earth alloys and $L1_0$-structure FePt and CoPt nanoparticles have superior permanent-magnet properties,[6–8] but an ever-increasing demand of rare-earth elements and the high cost of Pt intensify the search for rare-earth and Pt-free alloys.[9,10] Another important problem is that generally nanoparticles have low remanent magnetization M_r of only about 0.5 M_s due to the random distribution of easy axes and this limits potential use of nanoparticles in permanent magnets.[2,11,12] However, the easy-axis alignment process for the improvement of M_r/M_s using a magnetic field during the growth of nanoparticles is strongly hindered by the requirement of formation at high temperature (above 500 °C) for obtaining the desired crystalline ordering.[13,14]

In the present study, we have overcome the above-mentioned problems by producing rare-earth-free permanent-magnet nanoparticles ($HfCo_7$) using a single-step gas-aggregation-type cluster-deposition method without the requirement of a high-temperature thermal annealing and subsequently aligned their easy axes *via* applying a magnetic field, prior to deposition on substrates. Note that the $HfCo_7$ intermetallic phase can play a key role in the ongoing search for alternative permanent-magnet alloys due to its high T_c of about 600 K, J_s of above 10 kG, and non-cubic crystal structure.[15–19] The $HfCo_7$ phase, however, forms only at a single composition (12.5 at. % of Hf) and temperatures as high above 1000 °C under thermal equilibrium conditions. These limitations are major impediments in controlling the phase purity, crystalline ordering, and microstructure of bulk alloys, which affect their permanent-magnet properies.[15,16] In this regard, the non-equilibrium growth conditions of the cluster-deposition method are advantageous for the stabilization of metastable phases, and alloys requiring higher growth temperatures and with less symmetric crystal structures.[6,20,21]

The experimental setup used for depositing $HfCo_7$ nanoparticles, as schematically shown in Fig. 1, consists of a cluster-formation chamber having a direct current (DC) magnetron plasma-sputtering discharge with a water-cooled gas-aggregation chamber and a deposition chamber, where the substrate is kept at room temperature.[6] The Co-Hf composite target was sputtered at a high DC magnetron sputtering power ($P_{dc} = 200$ W) using a mixture of argon (Ar) and helium (He) as sputtering gas to form $HfCo_7$ nanoparticles in the gas-aggregation chamber, which were extracted as a collimated beam moving towards the substrate. Nanoparticles were deposited on single crystalline Si (001) substrates for superconducting quantum interference device (SQUID) magnetometer, energy dispersive x-ray analysis (EDX, JEOL JSM 840 A scanning electron microscope), and x-ray diffraction (XRD, Rigaku D/Max-B diffractometer) measurements. Carbon-coated copper grids were used as substrates for transmission electron microscopy (TEM, JEOL 2010 with an acceleration voltage of 200 kV) studies. For the fabrication of $HfCo_7$:Fe-Co nanocomposites, $HfCo_7$ nanoparticles were co-deposited along with soft Fe_xCo_{1-x} phase ($x = 0.65$) produced using another dc magnetron sputtering gun employed in the

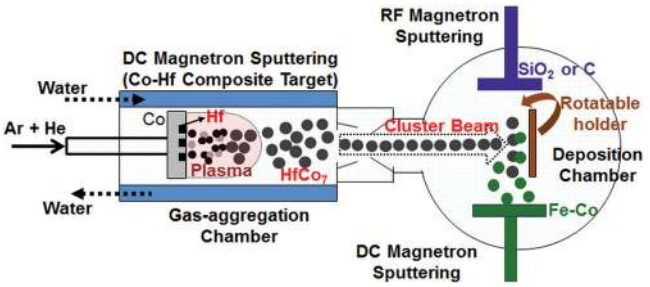

FIG. 1. A schematic illustration of the gas-aggregation-type cluster-deposition method used for the growth of $HfCo_7$ nanoparticles.

a)Author to whom correspondence should be addressed. Electronic mail: dsellmyer@unl.edu.

deposition chamber as shown in Fig. 1. During the deposition of nanocomposites, the substrate holder was rotated by about 20° to face both cluster beam and Fe-Co flux. The volume fraction of the soft phase was controlled by varying the deposition rate of $HfCo_7$ nanoparticles and Fe-Co. Nanoparticle samples were coated with a protective cap layer (about 3 nm) such as SiO_2 immediately after deposition using a RF sputtering gun employed in the deposition chamber.

We have deposited two types of nanoparticle samples: (i) randomly oriented nanoparticles in the absence of a magnetic field (labeled as unaligned nanoparticles) and oriented nanoparticles by applying a magnetic field to nanoparticles using a set of permanent magnets before deposition (labeled as aligned nanoparticles), which will be discussed later. We also have prepared bulk $HfCo_7$ alloys for comparing the structural and magnetic properties of nanoparticles. For this, high-purity Co and Hf of compositions corresponding to $HfCo_7$ (12.5 at. %. of Hf) were mixed homogeneously using a conventional arc-melting method and subsequently melt spun to obtain bulk $HfCo_7$ ribbons. The rapid cooling during the melt spinning process is advantageous to have good control over the phase purity and microstructure in the bulk $HfCo_7$ alloys.

XRD measurements were used to investigate the crystal structure of $HfCo_7$. Note that the bulk $HfCo_7$ is reported to form one of the following structures: tetragonal or orthorhombic.[15,17–19] In the present study, we first used TOPAS (Total Pattern Analysis Solution, Bruker AXS) to index the XRD pattern of the bulk $HfCo_7$ alloys (curve (i) in Fig. 2(a)) by assuming the above-mentioned crystal structures. The positions of the experimental XRD peaks (curve (i) in Fig. 2(a)) show good agreement with the XRD peak positions using TOPAS (black-dotted vertical lines in Fig. 2(a)) for an orthorhombic structure having lattice parameters of about $a = 4.7189$ Å; $b = 4.2783$ Å, and $c = 8.0705$ Å. Similarly, the XRD pattern of the unaligned $HfCo_7$ nanoparticles (curve (ii) in Fig. 2(a)) shows the most intense diffraction peaks corresponding to (002), (200), and (202) as observed in the case of bulk $HfCo_7$ alloys.

Some of the low-intensity diffraction peaks are weak or not visible in the XRD pattern of the unaligned $HfCo_7$ nanoparticles (curve (ii) in Fig. 2(a)) due to comparatively low absolute intensities. In addition, the diffraction peaks corresponding to (202) and (004) separated only by a small angular position are indistinguishable due to their breadth resulting from the nanoparticle size. Generally, the cluster-deposition method produces assemblies of single-crystalline nanoparticles of average particle size $d \leq 15$ nm with an rms standard deviation of $\sigma/d \leq 0.20$ and this depends on the gas flow rates, gas-aggregation length, and P_{dc}.[6] The size d for $HfCo_7$ nanoparticles was varied from about 4.8 to 12 nm by varying the flow rate of Ar (200 to 500 SCCM (standard cubic centimeter per minute)) and/or gas aggregation length (10 to 15 cm), while keeping P_{dc} (200 W) and flow rate of He (100 SCCM) as constants. For example, in the present study, TEM image of $HfCo_7$ nanoparticles (Fig. 2(b)) and corresponding particle-size histogram (inset of Fig. 2(b)) reveal $d = 8.3$ nm and $\sigma/d = 0.19$.

Magnetic properties of unaligned $HfCo_7$ nanoparticles were investigated by measuring the magnetization M as a function of applied magnetic field H from −70 to 70 kOe

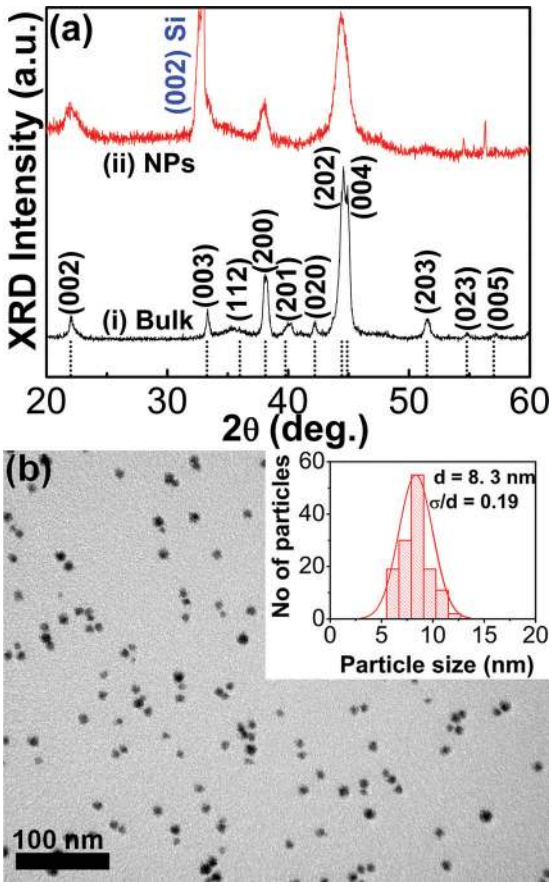

FIG. 2. (a) X-ray diffraction patterns of bulk $HfCo_7$ and unaligned $HfCo_7$ nanoparticles (NPs), where the estimated XRD peak positions corresponding to the orthorhombic structure using TOPAS are shown as black-dotted vertical lines. (b) Transmission electron microscope image of NPs. The corresponding particle-size histogram is given as an inset, where σ and d are the standard deviation and average particle size, respectively.

and also compared with that of bulk $HfCo_7$ alloys. $HfCo_7$ nanoparticles with $d = 4.8$ nm exhibit superparamagnetic behavior by showing a coercivity $H_c = 0$ at 300 K and blocking temperature of about 140 K in the zero-field-cooled magnetization curve (not shown here) and those having $d > 5$ nm always show ferromagnetic behavior. For example, *M-H* curves of the unaligned $HfCo_7$ nanoparticles having $d = 8.3$ nm measured at 10 K (blue curve) and 300 K (red curve) are shown along with the room-temperature *M-H* curve of the bulk $HfCo_7$ alloys (black curve) in Fig. 3(a). These results provide two important observations. First, M of both unaligned $HfCo_7$ nanoparticles and bulk alloys in Fig. 3(a) does not attain complete saturation even at $H = 70$ kOe, revealing a large value of magnetic anisotropy. The magnetic anisotropy constant K_1 was estimated by fitting the high field region of *M-H* curves using the law of approach to saturation method, widely used for randomly oriented nanoparticles.[12,22–24] This behavior is consistent with the observation of M_r/M_s of about 0.5 and nearly identical room-temperature in-plane and out-of-plane *M-H* curves of the unaligned $HfCo_7$ nanoparticles (not shown here).

The magnetization for random-anisotropy magnets near saturation (M_s) can be estimated from

$$M = M_s(1 - A/H^2) + \chi H. \quad (1)$$

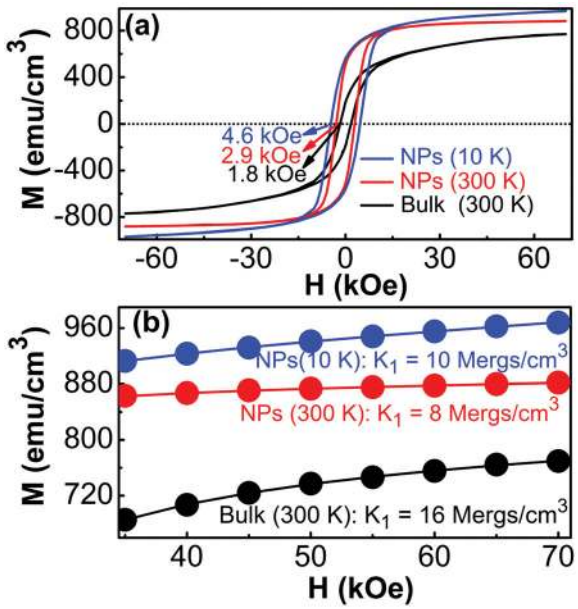

FIG. 3. (a) *M-H* curves of the unaligned $HfCo_7$ NPs measured at 10 K and 300 K and bulk alloy measured at 300 K. (b) An estimation of magnetic anisotropy constant K_1 from the high-field region of *M* vs. *H* curves using the law of approach to saturation method (see Refs. 12 and 22–24). The solid spheres and lines represent the corresponding experimental data and fitting, respectively.

In Eq. (1), χ is the high-field susceptibility and the constant *A* depends on the anisotropy constant K_1 as given by

$$A = \frac{4}{15}\frac{K_1^2}{M_s^2}. \quad (2)$$

The high-field region of *M* ($H \geq 30$ kOe) in Fig. 3(a) is fitted using Eq. (1) to estimate K_1 as shown in Fig. 3(b), where the experimental and fitted data are represented by solid spheres and lines, respectively. This evaluation shows that both $HfCo_7$ nanoparticles and bulk alloys have high anisotropies of about 10 Mergs/cm^3 as indicated in Fig. 3(b). $HfCo_7$ nanoparticles have a lower K_1 than bulk, presumably due to disorder and surface effects in nanoparticles.[11] Second, $HfCo_7$ nanoparticles exhibit H_c of 4.6 kOe at 10 K and 2.9 kOe at 300 K and J_s of about 10.9 kG, which are comparable with those of reported rare-earth alloy nanoparticles.[7,25–29] In addition, the room-temperature coercivity of $HfCo_7$ nanoparticles (2.9 kOe) is higher than that of bulk $HfCo_7$ alloys (1.8 kOe). In contrast, Co nanoparticles and bulk metal exhibit H_c less than 50 Oe and a low K_1 of about 5 Mergs/cm^3 (not shown here).

In the present study, $HfCo_7$ nanoparticles gain sufficient energy for crystallization from the collisions with the ions during the gas-aggregation process[20,21,30] and form the desired high-anisotropy crystal structure without a subsequent high-temperature annealing, which is normally required in the case of permanent-magnet alloys and nanoparticles.[7,8] Thus, it is possible to fabricate exchange-coupled nanocomposites using co-deposition method as discussed earlier without modifying the crystal structure, phase purity, and particle size of $HfCo_7$ nanoparticles. A Fe-Co target with $Fe_{65}Co_{35}$ composition (which has a high J_s of about 24 kG) was used to deposit Fe-Co soft phase. XRD pattern and *M-H* curve of the soft Fe-Co layer deposited in the absence of nanoparticle beam showed a body-centered cubic structure and soft magnetic properties: $H_c = 52$ Oe, $J_s = 22.5$ kG, and $M_r/M_s = 0.79$ at 300 K, respectively (not shown here).

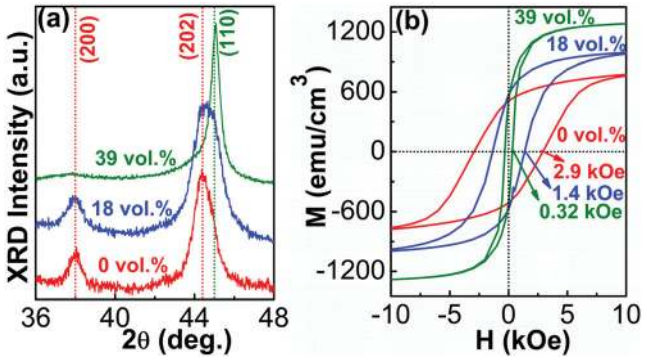

FIG. 4. The unaligned exchanged-coupled $HfCo_7$:Fe-Co nanocomposites with different volume fractions (vol. %) of soft Fe-Co phase: (a) X-ray diffraction patterns, where the red and green-dotted vertical lines represent the standard positions of diffraction peaks corresponding to $HfCo_7$ and Fe-Co, respectively. (b) The expanded room-temperature *M-H* curves.

The exchange coupling of hard magnetic nanoparticles with soft magnetic phases is expected to improve J_s.[31–36] XRD patterns and expanded room-temperature *M-H* curves of unaligned $HfCo_7$:Fe-Co nanocomposites having 0, 18, and 39 vol. % of soft Fe-Co phase are shown in Figs. 4(a) and 4(b), respectively. The variation of the Fe-Co soft phase in these nanocomposite samples is clearly evident from the changes in the relative intensities of XRD peaks corresponding to Fe-Co and $HfCo_7$ nanoparticles as shown in Fig. 3(a). The position of diffraction peaks corresponding to (200) and (202) of orthorhombic $HfCo_7$ and (110) of bcc FeCo are indicated by red and green-dotted vertical lines, respectively in Fig. 4(a). As compared to (200) and (202) diffraction peaks of $HfCo_7$ nanoparticles, the XRD peak corresponding to (110) of bcc Fe-Co is comparably intense for 18 vol. % of Fe-Co (blue curve) and becomes dominant on increasing Fe-Co content to 39 vol. % of Fe-Co (green curve) as shown in Fig. 4(a). Higher-resolution TEM images clearly show that 8.3 nm $HfCo_7$ nanoparticles are coated and surrounded by Fe-Co phase (not shown here).

The room-temperature *M-H* curve of unaligned $HfCo_7$ nanoparticles show $H_c = 2.9$ kOe and $J_s = 10.9$ kG at 300 K (red curve in Fig. 4(b)). $HfCo_7$:Fe-Co nanocomposites show an increase in J_s from 13.6 kG to as high as 16.6 kG on increasing Fe-Co fractions from 18 to 39 vol. %, but they exhibit decreasing H_c values of 1.4 and 0.32 kOe for 18 vol. % and 39 vol. % of Fe-Co, respectively as shown in Fig. 4(b). In ideal exchange-coupled nanocomposites, magnetic moments in both hard and soft phases are expected to switch coherently and the resultant H_c and J_s will be some average of the constituent phases. H_c is, however, expected to reduce substantially for nanocomposites having more than 20 vol. % of soft phase due to the propagation of domain walls.[31–36]

Although unaligned $HfCo_7$ nanoparticles and $HfCo_7$:Fe-Co nanocomposites have shown appreciable permanent-magnet properties, they exhibit a low M_r/M_s of about 0.5 due to the random distribution of easy axes. The isotropic nature of the hard phase has been observed to affect the energy products of nanocomposite permanent magnets.[31–33] For example,

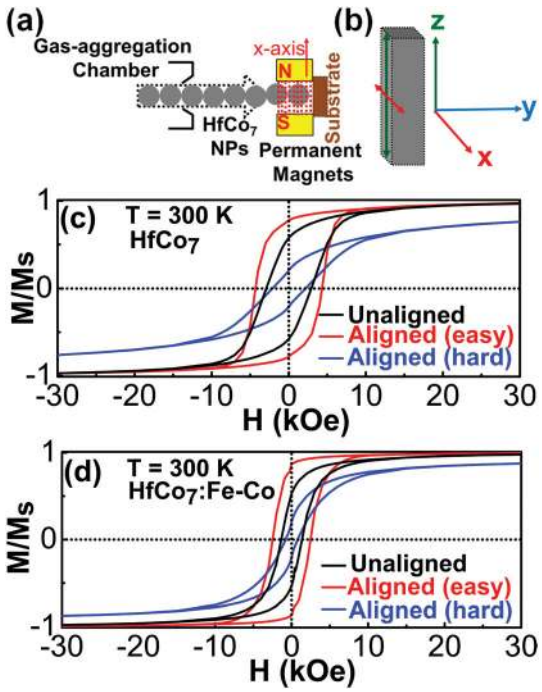

FIG. 5. Easy-axis alignment of $HfCo_7$ nanoparticles (NPs): (a) Schematic illustration of the alignment method using a set of permanent magnets (NS), prior to deposition on substrate, where the sputtering guns used for depositing Fe-Co soft phase and cap layer are not shown here. (b) Three dimensional view of the substrate is also given—in order to show the direction of the applied magnetic field (x-axis) used for alignment with respect to the substrate plane. The expanded room-temperature *M-H* curves of the aligned NPs measured along the easy (x-axis) and hard (y-axis) directions for (c) $HfCo_7$ NPS and (d) $HfCo_7$:Fe-Co nanocomposites with 18 vol. % of Fe-Co, whereas the *M-H* curves for the corresponding unaligned samples also are given for comparison.

the isotropic exchange-coupled Fe-Pt and Sm-Co—based nanocomposite magnets show $(BH)_{max}$ of about 20 MGOe, which is lower than the theoretical value of anisotropic $Nd_2Fe_{14}B$—based magnets (58 MGOe) and preferentially textured FePt-based composite thin films deposited on MgO substrates (54 MGOe).[31–33,37] In the case of nanoparticles, the requirement of high temperatures for obtaining the crystalline ordering of the hard phase hinders the easy-axis alignment process using a magnetic field. For example, thermal annealing of soft FePt nanoparticles having disordered face center cubic structure in a very large magnetic field to produce hard $L1_0$-ordering with aligned easy axes was unsuccessful, presumably due to the fact that the temperature required for higher ordering is above Curie temperature T_c.[13,14]

Since nanoparticle growth and crystallization of $HfCo_7$ nanoparticles occur directly during the gas-aggregation process in the present study, it is possible to align the easy axes by applying a magnetic field to $HfCo_7$ nanoparticles with a set of permanent magnets before deposition as shown in Fig. 5(a). By considering the substrate as a reference plane as shown in Fig. 5(b), $HfCo_7$ nanoparticles travel for a distance of 10 mm under the influence of a magnetic field of about 5 kOe applied along the x-axis, before landing on the substrate. In the present study, we have measured room-temperature *M-H* curves of two types of magnetically aligned samples: pure $HfCo_7$ nanoparticles (Fig. 5(c)) and $HfCo_7$:Fe-Co nanocomposites with 18 vol. % of Fe-Co (Fig. 5(d)). For comparison, *M-H* curves of the unaligned $HfCo_7$ and $HfCo_7$:Fe-Co with 18 vol. % of Fe-Co are also shown in Figs. 5(c) and 5(d), respectively.

TABLE I. Comparison of H_c and M_r/M_s at 300 K measured along easy (x-axis) and hard (y-axis) directions of the magnetically aligned $HfCo_7$ nanoparticles and $HfCo_7$:Fe-Co nanocomposites.

Sample	H_c (kOe)	M_r/M_s
Aligned $HfCo_7$	4.4 (easy)	0.78 (easy)
	1.9 (hard)	0.21 (hard)
Unaligned $HfCo_7$	2.9	0.57
Aligned $HfCo_7$:Fe-Co	2.5 (easy)	0.87 (easy)
	0.8 (hard)	0.21 (hard)
Unaligned $HfCo_7$:FeCo	1.4	0.53

H_c and M_r/M_s estimated from Figs. 5(c) and 5(d) are summarized in Table I. These results show an increase in H_c and M_r/M_s along the easy axis (x-axis) and a substantial reduction of those values along the hard axis (y-axis) in the aligned samples. Note that *M-H* loop of the aligned samples measured along the z-axis is identical to that measured along y-axis (not shown here). These results reveal an effective uniaxial alignment upon applying a magnetic field to $HfCo_7$ nanoparticles prior to deposition. We also have estimated the magnetic anisotropy constant by using the area under the complete *M-H* curves (from 0 to 70 kOe) of the aligned $HfCo_7$ nanoparticles along the easy and hard axes,[38] and this analysis yields a value of 9.0 Mergs/cm^3, in close agreement with 8.0 Mergs/cm^3 determined from the approach to saturation method. As shown in Table I, H_c and M_r/M_s of the aligned $HfCo_7$ and $HfCo_7$:Fe-Co samples measured along the easy axis are also higher than that of the corresponding unaligned samples.

In conclusion, we have succeeded in producing uniaxially aligned $HfCo_7$ nanoparticles and $HfCo_7$:Fe-Co nanocomposites at room temperature using a single-step cluster-deposition method. Structural analysis indicates that $HfCo_7$ likely crystallizes in the orthorhombic structure. $HfCo_7$ nanoparticles exhibit H_c (4.4 kOe), K_1 ($\sim$10 Mergs/cm^3), and J_s (10.8 kG) at 300 K, which are comparable with the magnetic properties of rare-earth alloy nanoparticles. An enhancement of J_s to as high as 16.6 kG was observed in $HfCo_7$:Fe-Co nanocomposites on varying Fe-Co concentration to 39 vol. %, although the coercivity is reduced as compared to $HfCo_7$ nanoparticles. This methodology also can be adopted easily to produce aligned nanoparticles of additional permanent-magnet alloys. The direct crystalline-ordering, *in situ* easy-axis alignment, and nanocomposite fabrication reported in the present study are important processing steps towards fabricating nanoparticle assemblies for next-generation nanocomposite magnets with improved performance.

This work is supported by Advanced Research Projects Agency-Energy (Grant No. DE-AR 0000046, B.B. and B.D.), US Department of Energy (Grant No. DE-FG02-04ER46152, D.J.S.), NSF-Materials Research Science and Engineering Center (Grant No. DMR-0820521, R.S.), and Nebraska Center for Materials and Nanoscience (V.R.S. and X.Z.L.). Thanks are due to Jeff Shield, Damien LeRoy, Z. Sun, and P.K. Sahota for helpful discussions.

[1]N. A. Frey, S. Peng, K. Cheng, and S. Sun, Chem. Soc. Rev. **38**, 2532 (2009).
[2]B. Balamurugan, D. J. Sellmyer, G. C. Hadjipanayis, and R. Skomski, Scr. Mater. **67**, 542 (2012).
[3]D. Weller and T. McDaniel in *Advanced Magnetic Nanostructures*, edited by D. J. Sellmyer and R. Skomski (Springer, Berlin, 2006), p. 295.
[4]G. Reiss and A. Hütten, Nature Mater. **4**, 725 (2005).
[5]D. J. Sellmyer, Nature (London) **420**, 374 (2002).
[6]B. Balasubramanian, R. Skomski, X. Z. Li, S. R. Valloppilly, J. E. Shield, G. C. Hadjipanayis, and D. J. Sellmyer, Nano. Lett. **11**, 1747 (2011).
[7]S. Sun, C. B. Murray, D. Weller, L. Folks, and A. Moser, Science **287**, 1989 (2000).
[8]D. Alloyeau, C. Ricolleau, C. Mottet, T. Oikawa, C. Langlois, Y. Le Bouar, N. Braidy, and A. Loiseau, Nature Mater. **8**, 940 (2009).
[9]N. Jones, Nature (London) **472**, 22 (2011).
[10]R. Skomski, J. E. Shield, and D. J. Sellmyer, *Magnetic Technology International* (UKIP Media and Events Ltd., 2011), p. 26.
[11]Y. Xu, M. L. Yan, J. Zhou, and D. J. Sellmyer, J. Appl. Phys. **97**, 10J320 (2005).
[12]E. Kneller, *Ferromagnetism* (Springer, Berlin, 1962).
[13]S. Kang, Z. Jia, S. Shi, D. E. Nikles, and J. W. Harrell, Appl. Phys. Lett. **86**, 062503 (2005).
[14]S. Kang, S. Shi, Z. Jia, G. B. Thompson, D. E. Nikles, J. W. Harrell, D. Li, N. Poudyal, V. Nandwana, and J. P. Liu, J. Appl. Phys. **101**, 09J113 (2007).
[15]K. H. J. Buschow, J. Appl. Phys. **53**, 7713 (1982).
[16]Y. Shimada and H. Kojima, J. Appl. Phys. **53**, 3156 (1982).
[17]B. G. Demczyk and S. F. Cheng, J. Appl. Cryst. **24**, 1023 (1991).
[18]S. C. Bedi and M. Forker, Phys. Rev. B **22**, 14948 (1993).
[19]H. Okamoto, *Phase Diagram of Binary Alloys* (ASM, Materials Park, 2000), p. 248.
[20]H. Haberland, M. Karrais, M. Mall, and Y. Thurner, J. Vac. Sci. Technol. A **10**, 3266 (2000).
[21]J. M. Qiu, J. Bai, and J. P. Wang, Appl. Phys. Lett. **89**, 222506 (2006).
[22]G. C. Hadjipanayis, D. J. Sellmyer, and B. Brandt, Phys. Rev. B **23**, 3349 (1981).
[23]A. Franco, Jr. and F. C. E. Silva, Appl. Phys. Lett. **96**, 172505 (2010).
[24]X. Liu, J. Bai, F. Wei. Z. Yang, S. Takei, A. Morisako, and M. Matsumoto, J. Appl. Phys. **87**, 6875 (2000).
[25]V. M. Chakka, B. Altuncevahir, Z. Q. Jin, and J. P. Liu, J. Appl. Phys. **99**, 08E912 (2006).
[26]T. Matsushita, T. Iwamoto, M. Inokuchi, and N. Toshima, Nanotechnology **21**, 095603 (2010).
[27]B. Balamurugan, R. Skomski, X. Z. Li, G. C. Hadjipanayis, and D. J. Sellmyer, J. Appl. Phys. **111**, 07B527 (2012).
[28]C. H. Chen, S. J. Knutson, Y. Shen, R. A. Wheeler, J. C. Horwath, and P. N. Barnes, Appl. Phys. Lett. **99**, 012504 (2011).
[29]N. G. Akdogan, G. C. Hadjipanayis, and D. J. Sellmyer, Nanotechnology **21**, 295705 (2010).
[30]M. M. Patterson, A. Cochran, J. Ferina, X. Rui, T. A. Zimmerman, Z. Sun, M. J. Kramer, D. J. Sellmyer, and J. E. Shield, J. Vac. Sci. Technol. B **28**, 273 (2010).
[31]H. Zeng, J. Li, J. P. Liu, Z. L. Wang, and S. Sun, Nature (London) **420**, 395 (2002).
[32]X. Rui, J. E. Shield, Z. Sun, Y. Xu, and D. J. Sellmyer, Appl. Phys. Lett. **89**, 122509 (2006).
[33]Y. Zhang, M. J. Kramer, C. Rong, and J. P. Liu, Appl. Phys. Lett. **97**, 032506 (2010).
[34]R. Coehoorn, D. B. de Mooij, and C. J. de Waard, J. Magn. Magn. Mater. **80**, 101 (1989).
[35]E. F. Kneller and R. Hawig, IEEE Trans. Magn. **27**, 3588 (1991).
[36]R. Skomski and J. M. D. Coey, Phys. Rev. B **48**, 15812 (1993).
[37]Y. Liu, T. George, R. Skomski, and X. Z. Li, Appl. Phys. Lett. **99**, 172504 (2011).
[38]D. J. Sellmyer and Z. S. Shan, in *Science and Technology of Nanostructured Magnetic Materials*, edited by G. Hadjipanayis and G. A. Prinz (Plenum, New York, 1991), p. 151.